Self-pulsing 10^4 A cm^{-2} current density discharges in dielectric barrier Al/Al_2O_3 microplasma devices

D. Yarmolich,[1] Ya. E. Krasik,[1,a)] E. Stambulchik,[2] V. Bernshtam,[2] J. K. Yoon,[3] B. Herrera,[3] S.-J. Park,[3] and J. G. Eden[3]
[1]*Department of Physics, Technion, Haifa 32000, Israel*
[2]*Department of Physics, Weizmann Institute of Science, Rehovot 76100, Israel*
[3]*Department of Electrical and Computer Engineering, University of Illinois, Urbana, Illinois, 61801, USA*

(Received 27 September 2008; accepted 10 December 2008; published online 6 January 2009)

Excitation of Al/Al_2O_3 microplasma devices with 50 μs, 800 V pulses produces, in Ar/H_2 gas mixtures at 600 Torr, ~6 A current pulses with a duration of ~30 ns. Corresponding to peak current and power densities of $\sim 10^4$ A/cm^2 and ~2.5 GW/cm^3, respectively, these pulses are generated in a 10 μs burst in which the voltage self-pulses at a repetition frequency of ~3 MHz. Analysis of the H_α, H_β, and Ar II emission line profiles yields a plasma density of $\sim 10^{17}$ cm^{-3}, and the emission of O IV ions suggests the presence of energetic electrons. Images of the microplasma indicate that the plasma is initiated by surface flashover and extends ~200 μm outside the microcavity. © *2009 American Institute of Physics*. [DOI: 10.1063/1.3064159]

During the past decade, experimental and computational studies of microcavity plasmas have explored the physical mechanisms governing their unique operating parameters.[1] Distinguishing characteristics of microplasmas include, for example, gas or vapor pressures near 1 atm and power density loadings of up to 100 kW/cm^3. Devices having microcavity dimensions in the 10–200 μm range have been investigated with dc, steady-state ac, and bipolar pulsed excitation, and the maximum value of the electron density n_e reported to date is $\lesssim 10^{16}$ cm^{-3} (Refs. 1–6). Potential applications of microplasmas as pixellated, short wavelength radiation or electron sources, in particular, hinge on the maximum values of electron density and temperature that are attainable.

This letter reports several fundamental properties of Al/Al_2O_3 microplasma devices[7,8] driven by 50 μs pulses. When operating in 95% Ar/5% H_2 gas mixtures, 100 μm diameter microcavity devices produce a 10 μs burst of 30 ns current pulses having a peak value of ~6 A, which corresponds to a current density of $j_e \approx 10^4$ A/cm^2 and a specific power loading of ~2.5 GW/cm^3. Emission spectroscopy of Stark broadened Ar ion and hydrogen atom transitions shows $n_e = (3.5 \pm 0.5) \times 10^{17}$ cm^{-3}.

The experiments were conducted with Al/Al_2O_3 microplasma devices having parabolic cross-sectional microcavities[8] with an emitting aperture of 200 μm. Each device comprises two microcavities formed in nanoporous alumina (Al_2O_3) and Al ring electrodes buried 20 μm below the microcavity surface. These electrode surfaces are conformal to the microcavity wall and azimuthally symmetric. All dimensions of the microplasma device are controlled within a tolerance of ±2% using a sequence of wet electrochemical processes. After aligning the larger of the two microcavities [having an emitting (upper) aperture of 200 ± 3 μm] with respect to the lower parabolic cavity such that their axes are collinear, the microcavities are bonded. The thickness of this double cavity structure is 150 μm. Further details regarding the fabrication processes for these devices can be found in Ref. 8.

Devices were installed in an experimental chamber that was evacuated and subsequently backfilled with a 95% Ar/5% H_2 gas mixture having a total pressure (p_T) of 600–700 Torr. Driving voltage pulses having a duration of 50 μs were generated by a pulser circuit based on a 2 nF capacitor charged to ~800 V and an electronic switch. Delivery of these pulses to the microplasma device through an ~1 mH inductor and a ~1 m length of coaxial cable results in the waveform in Fig. 1(a) recorded at a background pressure of 0.1 Torr in the chamber. Under these conditions, plasma is not generated in the microcavity, the damped sinusoid exhibits a period of ~4 μs, and the maximum voltage impressed on the device is ~900 V. If an Ar/H_2 gas mixture with p_T = 600 Torr is admitted to the chamber, plasma ignition occurs when the voltage magnitude reaches ~400 V. As illustrated in Fig. 1(b), breakdown is followed immediately by an ~10 μs period in which self-pulsing of both the voltage and current is observed. Operation in this burst mode ceases abruptly after 10 μs, a time period that is not noticeably altered if the inductance in the pulse delivery circuitry is varied over the 0.01–20 mH range and the generator capaci-

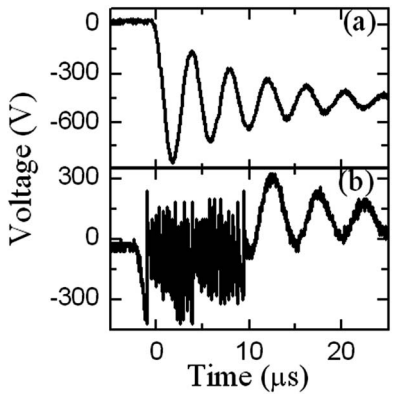

FIG. 1. Voltage waveforms representative of those recorded for a microcavity plasma device: (a) in vacuum (i.e., in the absence of plasma) and (b) when plasma is generated in an Ar/5% H_2 mixture at 600 Torr.

a)Electronic mail: fnkrasik@physics.technion.ac.il.

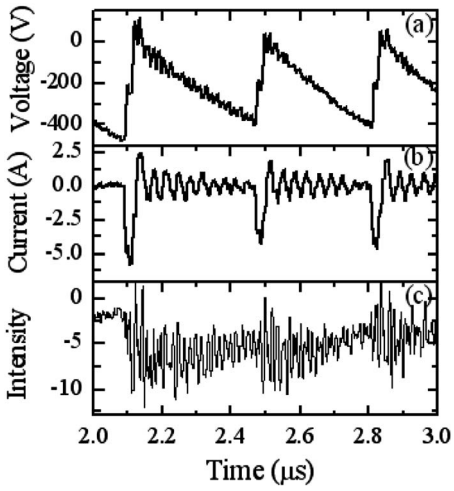

FIG. 2. Expanded views of (a) voltage, (b) current, and (c) relative visible emission intensity waveforms, illustrating the generation of current pulses having a temporal width of ~30 ns, peak values of 5–6 A, and a repetition frequency of ~3 MHz.

tance is increased up to 10 nF. Expanded views of a 2 μs segment of the voltage, current, and plasma emission waveforms (the latter recorded with a photomultiplier) are presented in Figs. 2(a)–2(c), respectively. In each cycle of the self-pulsing period, the voltage rises linearly over ~400 ns to −400 V and subsequently collapses to almost zero in ~30 ns. The rapid fall in the voltage is accompanied by a current pulse having a duration of also ~30 ns and a peak value of 6 A, which corresponds to a current density of ~6×10^4 A/cm^2. Optical emission from the microcavity generally follows the voltage waveform with the strongest intensity observed during the 30 ns current pulse and a precipitous decline thereafter.

Spatially and temporally resolved images of the plasma emission were also recorded with a 4QuikE framing camera coupled to a microscope. Figure 3 is a sequence of images, obtained with a spatial resolution of 3 μm/camera pixel, of the microplasma emission intensity observed end-on [Figs. 3(b)–3(d)] and at a right angle to the microcavity axis [side view: Figs. 3(f)–3(h)] for Ar/H_2 mixtures at p_T=600 Torr. For these measurements, the framing camera was triggered at several delay times (Δt) with respect to the tenth current pulse of Fig. 1(b)—which occurs approximately midway into the 10 μs burst—and the camera gate width was set at 30 ns. It is evident from the end-on images [Fig. 3(b)] that plasma formation is initiated inside the cavity at the onset of the current pulse by surface flashover. Raising the Ar/H_2 gas mixture pressure to 700 Torr leads to a decrease in the initial spatial extent of the plasma within the microcavity. As time progresses, plasma fills the cavity cross section [Δt=20 ns, Fig. 3(c)] and the visible emission from the plasma falls quickly thereafter [Fig. 3(d), Δt=60 ns]. At Δt=150 ns, the plasma emission is no longer detectable. Side view images [Figs. 3(e)–3(h)] reveal the plasma formation outside the microcavity as well. Approximately circular with a maximum diameter of 200 μm, the plume remains in the vicinity of the microcavity aperture throughout the plasma life cycle.

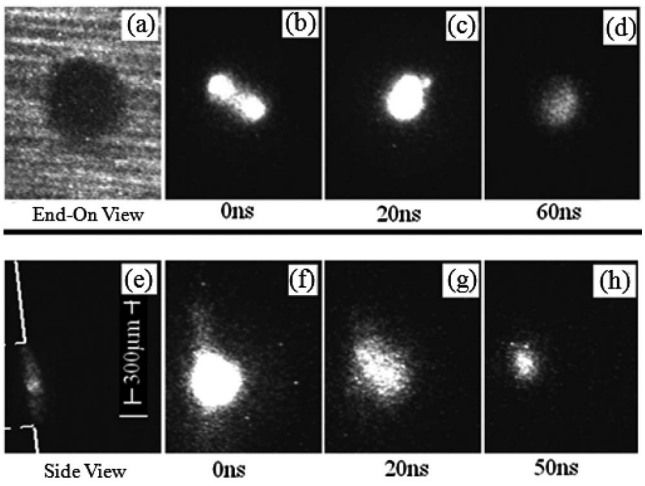

FIG. 3. Sequence of optical micrographs showing (a) an end-on (plan) view of the microcavity; [(b)–(d)] spatially resolved emission at Δt=0, 20, and 60 ns; (e) side view of the cavity (with the aperture outlined in white and the spatial scale indicated); and [(f)–(h)] spatially resolved emission profiles acquired for Δt=0, 20, and 50 ns.

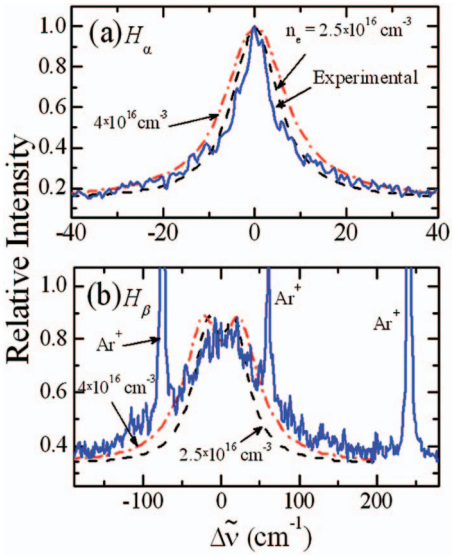

FIG. 4. (Color) Comparison of the measured and calculated spectral profiles for the H_α and H_β emission lines. Line profiles calculated for electron densities (n_e) of 2.5×10^{16} cm^{-3} and 4×10^{16} cm^{-3} are illustrated by the blue and red curves, respectively. The experimental spectra are in black. Three Ar II emission lines are also evident in the H_β spectrum in the lower panel.

To estimate the microplasma peak electron density, optical emission spectra were recorded with the framing camera coupled with a Bruker 500 imaging spectrometer having a resolution of 0.02 nm/pixel. Throughout these experiments, the spatial resolution of the collection optics/framing camera system was decreased to 200 μm, and the camera gate width was set at 10 μs to coincide with the duration of the burst mode. Stark broadening of the H_α and H_β lines was first examined and representative spectra are given in Figs. 4(a) and 4(b), respectively. Line profiles were calculated by the approach described in Ref. 9 that accounts for the dynamics of both electrons and ions in the plasma. If the time-averaged electron temperature is assumed to be T_e=5 eV, then the best fit of the simulations to the wings of the experimental spectral profiles yields $n_e\sim4\times10^{16}$ cm^{-3} (the red curves in Fig. 4).[10] However, the central part of both profiles is better reproduced by a lower value of $n_e\sim2.5\times10^{16}$ cm^{-3} (the blue curves in Fig. 4). Let us note that for this range of n_e, the H_α and H_β line shapes were found to be insensitive to T_e, a result in agreement with studies.[11]

Similar measurements and calculations for the 480.60, 484.78, and 487.98 nm lines of the Ar II ion indicate a significantly denser plasma. These atomic transitions [shown in Fig. 4(b)] were chosen for analysis partially because they lie in an uncongested spectral region, allowing one to invoke a Lorentzian line shape and to use tabulated values of Stark broadening.[12] We note that the 480.60 and 484.78 nm Ar II lines are components of the same multiplet and, thus, are expected to have almost identical Stark widths. In contrast, the 487.98 nm transition belongs to another multiplet, which exhibits a ~30% stronger Stark effect.[12] Experimental linewidths are indeed consistent with both considerations, thereby confirming that the Stark effect is the primary line-broadening mechanism. A comparison of the experimental and calculated line shapes yields $n_e=(3.5\pm0.5)\times10^{17}$ cm^{-3} or almost an order of magnitude higher than the values indicated by the H_α and H_β transitions.

The apparent inconsistency in the values of n_e estimated from measurements of Stark broadening of H and Ar II spectral lines can be understood in terms of the different temporal histories of these two species during the 10 μs camera exposure time. Collisional-radiative modeling,[11] for example, has shown that for $n_e\geq10^{16}$ cm^{-3} and $T_e\approx5$ eV, the H number density decreases by a factor of three in 30 ns as a result of ionization. The loss of Ar II by ionization, however, is considerably slower owing to the large ionization potential (27.6 eV). Thus, it appears that the H_α and H_β profiles in Fig. 4 are emitted when n_e is low, whereas the preponderance of the Ar II emission was generated when n_e was at or near its peak value.

Other spectral lines, emitted by Ar III, Ar IV, Al I, Al II, O II, and O IV, were also investigated. The time dependence of the Al I emission intensity at 309.2 nm, for example, shows a maximum at ~6 μs. Let us note that strong emission from O IV suggests the presence of energetic electrons in the plasma. Indeed, time-dependent collision radiative modeling of a Maxwellian plasma with $n_e=10^{17}$ cm^{-3} and $T_e=5$ eV shows that for a discharge duration of 30 ns, only ~6% of Ar and ~10^{-2}% of O atoms are triply ionized.

One concludes that the peak electric field amplitude ($E\sim30$ kV/cm) in the microcavity initiates dielectric surface flashover, forming within a few nanoseconds a dense plasma in the form of a narrow channel. The surface flashover plasma density can be estimated as $n_e=j_e/(0.25eV_e)\approx3.6\times10^{11}j_e\times T_e^{-1/2}$ cm^{-3}, where $V_e\approx6.8\times10^7\sqrt{T_e}$ cm/s is the electron thermal velocity.[13] Thus, for the range in current density $j_e\sim(10^4-10^5)$ A/cm^2 and $T_e\sim(1-10)$ eV, n_e will lie in the interval of $10^{16}-10^{17}$ cm^{-3}, which is consistent with spectroscopic measurements. The plasma conductivity can be estimated as[13] $\sigma=2.8\times10^{-4}n_e(n_n\Sigma V_e)^{-1}\approx28$ Ω^{-1} cm^{-1}, where $\Sigma\approx10^{-16}$ cm^2 is the electron-neutral collision cross section and $n_n\approx2\times10^{19}$ cm^{-3} is the neutral density. Taking into account that during the discharge, the average electric field $E<10^4$ V/cm, one obtains the discharge current density $j_e=\sigma E<3\times10^5$ A/cm^2, which agrees satisfactorily with the estimates based on saturation current density.

Following flashover, the plasma fills the cavity entirely and forms a glow discharge plasma bubble. After the termination of a 30 ns current pulse, charged particles in the plasma deplete the charge on the dielectric barrier. Indeed, the value of the electrode charge obtained as an integral of the discharge current was found to be decreasing in time between two successive discharge current pulses. The plasma decays until the capacitor formed by the device electrodes and the coaxial cable is again charged to the breakdown voltage. The plasma recombination time is $\tau_p\approx10^{26}n_e^{-2}T_e^{9/2}$, which is a few nanoseconds for $n_e>10^{16}$ cm^{-3} but is $>10^{-4}$ s for $n_e\leq10^{13}$ cm^{-3}.[13] We conclude that the plasma does not decay completely between current pulses. When the density of this plasma exceeds ~10^{14} cm^{-3}, the plasma Debye length becomes smaller than the microcavity diameter. The result is a screening of the electric field within the microcavity, which suppresses surface flashover and transitions the plasma from self-pulsing to a conventional mode of operation.

In summary, driving 100 μm diameter Al/Al_2O_3 microcavity plasma devices with 50 μs, 800 V pulses produces a ~10 μs burst of 6 A, ~30 ns current pulses. The power and energy densities in the microcavity reach ~2.5 GW/cm^3 and 0.3 kJ/cm^3, respectively, values that are considerably beyond those characteristic of previous microplasmas, irrespective of the mode of operation. The devices reported here extend the parameter range available to microplasmas and suggest the feasibility of realizing arrays of bright, multiampere electron sources.

One of us (J.G.E.) gratefully acknowledges the support of the U.S.–Israel Educational Foundation and the Air Force Office of Scientific Research, as well as the hospitality of the Department of Physics at the Technion, during the completion of this work.

[1] K. H. Becker, K. H. Schoenbach, and J. G. Eden, J. Phys. D **39**, R55 (2006).
[2] S.-J. Park, J. Chen, C. J. Wagner, N. P. Ostrom, C. Liu, and J. G. Eden, IEEE J. Sel. Top. Quantum Electron. **8**, 139 (2002).
[3] K. Tachibana, IEEEJ Trans. **1**, 145 (2006).
[4] F. Iza, G. J. Kim, S. M. Lee, J. K. Lee, J. L. Walsh, Y. T. Zhang, and M. G. Kong, Plasma Processes Polym. **5**, 322 (2008).
[5] M. J. Kushner, J. Appl. Phys. **95**, 846 (2004).
[6] O. Sakai, Y. Kishimoto, and K. Tachibana, J. Phys. D **38**, 431 (2005).
[7] S.-J. Park, K. S. Kim, and J. G. Eden, Appl. Phys. Lett. **86**, 221501 (2005).
[8] K. S. Kim, T. L. Kim, J. K. Yoon, S.-J. Park, and J. G. Eden, Appl. Phys. Lett. (submitted).
[9] E. Stambulchik and Y. Maron, J. Quant. Spectrosc. Radiat. Transf. **99**, 730 (2006).
[10] M. Moselhy, I. Petzenhauser, K. Frank, and K. H. Schoenbach, J. Phys. D **36**, 2922 (2003).
[11] M. A. Gigosos and V. Cardeñoso, J. Phys. B **29**, 4795 (1996).
[12] N. Konjević, J. Labat, Lj. Ćirković, and J. Purić, Z. Phys. **235**, 35 (1970).
[13] Yu. P. Raizer, *Gas Discharge Physics* (Springer, New York, 1997).